Korean J. Chem. Eng., 33(4), 1380-1390 (2016)
DOI: 10.1007/s11814-015-0275-8

pISSN: 0256-1115
eISSN: 1975-7220

Novel ion-exchange nanocomposite membrane containing in-situ formed FeOOH nanoparticles: Synthesis, characterization and transport properties

Farhad Heidary*,†, Ali Reza Khodabakhshi,†, and Ali Nemati Kharat***

*School of Chemistry, College of Science, University of Tehran, Tehran, Iran
**Department of Chemistry, Faculty of Science, Arak University, Arak 38156-8-8349, Iran
(*Received 19 June 2015 • accepted 11 December 2015*)

Abstract−A new type of cation-exchange nanocomposite membrane was prepared via in-situ formation of FeOOH nanoparticles in a blend containing sulfonated poly (2,6-dimethyl-1,4-phenylene oxide) and sulfonated polyvinylchloride by a simple one-step chemical method. Prepared nanocomposite membranes were characterized using Fourier transform infrared spectroscopy, scanning electron microscopy and X-ray diffraction. The SEM images showed uniform dispersion of FeOOH nanoparticles throughout the polymeric matrices. The effect of additive loading on physicochemical and electrochemical properties of prepared cation-exchange nanocomposite membranes was studied. Various characterizations showed that the incorporation of different amounts of FeOOH nanoparticles into the basic membrane structure had a significant influence on the membrane performance and could improve the electrochemical properties.

Keywords: Nanocomposites, Cation-exchange Membranes, FeOOH Nanoparticles, Transport Number, Electrochemical Properties

INTRODUCTION

The significance of membrane processes for the treatment of wastewater and drinking water is still growing. The expense of membranes continues to decrease and it is possible to predict that membranes will be in extensive use in water treatment processes. Ion-exchange membranes, which are one of the most advanced membranes, have been used in various industrial separation processes [1]: chlor-alkali industry, electrodialysis (ED), electro-membrane reactors, electro-deionization and diffusion dialysis [2-5]. Recently, the number of industrial applications has gained increasing interest. The use of ion-exchange membranes in fuel cells and separation processes stands out owing to their considerable environmental and economical advantages [6,7]. The features of ion-exchange membranes determine to a great extent the performance of electrodialysis processes. These membranes have charged groups attached to their structure, which under the influence of an electric field allows the permeation of ions with opposite charge through the membrane and rejects ions with the same charge sign [6]. The development of ion-exchange membranes with improved permselectivity, lower electrical resistance and suitable chemical and thermal stability at lower cost is one of the most necessary requirements [8,9]. However, the evaluation of new materials for membrane fabrication opens up the opportunity for further related processes development [10]. The composite membranes represent the essential properties of organic polymeric matrix and inorganic fillers and put forward specific advantages for the fabrication of new membranes with suitable separation performance [11-14]. Thus, organic-inorganic composite materials have attracted more concern in membrane fabrication. Many studies explain the synthesis of adsorptive membranes via polymer blending and additive loading procedures using nanomaterials such as metal oxide nanoparticles to enhance membranes performance for wastewater treatment [15,16]. The polymers are considered the important materials in fabrication of composite membranes due to the benefits of their desirable membrane forming ability, flexibility and reasonable cost. Poly (2,6-dimethyl-1,4-phenylene oxide) (PPO) is an aryl compound with excellent membrane-forming properties, suitable thermal and chemical stability [17]. Among the PPO derivatives, aryl substituted sulfonated PPO (SPPO) is an appropriate structure which is used as a membrane for reverse osmosis, gas separation, ultra-filtration and cation-exchange membranes [18-21]. However, SPPO contains plenty of -SO_3Na groups and is highly hydrophilic, so, it can swell strongly in water if the degree of sulfonation is above 28%. The dimensional instability of SPPO is a disadvantage which prevents its practical applications in fuel cells and electro-membrane processes [17]. One attractive procedure for improving the membrane properties (e.g., water swelling and dimensional stability) is blending of a mechanical and dimensional stable material into hydrocarbon based polymers; thus, blending of two polymers such as sulfonated polyvinyl chloride (SPVC) and SPPO can generate a structure with novel properties and the membranes are expected to be ion-exchangeable and dimensionally stable. Polyvinyl chloride (PVC) is an outstanding material because of its high mechanical strength, reasonable cost and excellent chemical properties (resistance against acid, alkali and organic solvents) [22]. The PVC-SO_3H structures have applications as a sorbent, based on cation-

†To whom correspondence should be addressed.
E-mail: heidary.farhad@yahoo.com, farhad.heidary@ut.ac.ir, a_khodabakhshi@yahoo.com, a-khodabakhshi@Araku.ac.ir

exchange and hydro-phobicity simultaneously [23]. FeOOH is a type of abundant mineral and one of the most durable iron oxide under ambient conditions; it exists chiefly in soil, sediment and iron ore [24]. It can be synthesized by a facile method [25-28] and easy to incorporate with other components because of its numerous surface hydroxyl groups [29]. Moreover, FeOOH has attracted great interest due to its excellent reactivity, unique adsorption, ion exchange capacity, environmental safety, low cost and catalytic properties [30]. However, recycling of FeOOH nanoparticles is difficult after using. Hence, how to improve the recycle abilities and prevent agglomeration is important for the utilization of FeOOH in applicable conditions. To solve the problem and to modify the adsorption effect of the nanoparticles, FeOOH nanoparticles are typically dispersed on a high surface area carrier [25].

Preparing the new type of cation-exchange nanocomposite membranes with appropriate physicochemical properties for application in electrodialysis process was the main aim in this experimental work. FeOOH nanoparticles were in situ formed in polymeric matrix, and FeOOH/SPPO+SPVC nanocomposites were synthesized using the one-step synthetic method. Sonication was employed in membrane preparation to achieve better homogeneity in the matrix and also to obtain better electrochemical properties and mechanical integrity. Currently, no reports have considered incorporating FeOOH nanoparticles into cation-exchange membranes. The effect of FeOOH nanoparticles loading on the physicochemical properties of prepared cation-exchange nanocomposite membranes was studied and evaluated. During this experiment, sodium chloride solutions with various concentrations were employed for membrane characterization. The results are applicable for electro-membrane processes especially in electro-dialysis process for waste water treatment and water recovery.

EXPERIMENTAL

1. Materials and Instruments

Polyvinylchloride (PVC) was purchased from BIPC, Iran, grade S-7054. Poly (2,6-dimethyl-1,4-phenylene oxide) (PPO) with inherent viscosity of 0.57 dl/g in chloroform at 25 °C was obtained from Institute of Chemical Engineering of Beijing (China); SPPO was prepared by sulfonation of PPO according to the literature [31].

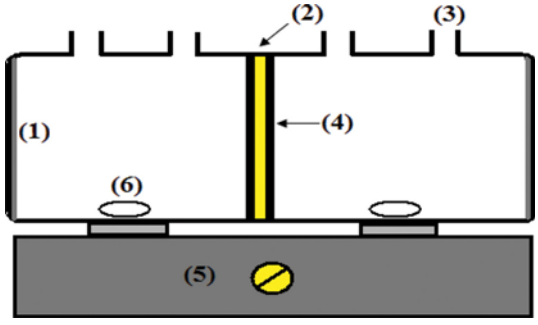

Fig. 1. Schematic diagram of test cell.

(1) Pt electrode
(2) Membrane
(3) Orifice
(4) Rubber ring
(5) Stirrer
(6) Magnetic bar

Tetrahydrofuran (THF) LR grade as solvent, sodium chloride and sulfuric acid (98%), $FeCl_3 \cdot 6H_2O$ and NH_3 were supplied from Merck Company. Throughout the experiment, distilled water was used.

The test cell for evaluation of membrane electrochemical properties is shown in Fig. 1. The cell consists of two cylindrical sections (vessel, each 140 cm^3) made of Pyrex glass which are separated by a membrane. The membrane was fixed between rubber rings. One side of each vessel was sealed by Pt electrode supported with a fragment of Teflon (Polytetrafluoroethylene) and the other side was equipped with a piece of porous medium to support the membrane. There are two orifices on the top of each compartment for feeding and sampling purposes. To minimize the influence of boundary layer during experiments and to diminish the concentration polarization on the vicinity of membrane's surface, both sections were stirred vigorously by magnetic stirrers (Model: Velp Sientifica Multi 6 stirrer); the membrane area was also 13.85 cm^2. The experiments were randomly repeated in triplicate, and the desirable confidence limit (around 96%) was attained.

XRD patterns were recorded by a Philips X-ray diffractometer using Ni-filtered Cu Ka radiation. Morphological investigations of the membranes were carried out using scanning electron microscopy (SEM) from Philips Company at an acceleration voltage of 25 kV. The samples were sputtered with gold to obtain a conductive surface and were investigated with the microscope. FT-IR spectra were recorded on Galaxy series FTIR5000 spectrophotometer.

2. PVC Sulfonation and Preparation of Cation-exchange Nanocomposite Membranes

Sulfonated polyvinylchloride (SPVC) was prepared by sulfonation of PVC according to the literature. To sulfonate PVC, at first, PVC powder was soaked in 1,2-dichloroethane for 4 h to swell the polymer. The pre-swollen PVC was immersed in sulfuric acid (98%) for another 4 h at 60 °C. After the reaction, the polymer was washed with 400 ml of deionized water to remove excess sulfuric acid and then with acetonitrile to eliminate any possible impurities. Then, the cleaned PVC-SO_3H polymer was dried at room temperature.

The cation-exchange nanocomposite membranes were prepared by casting solution technique via in-situ formation of FeOOH nanoparticles in the polymeric matrix. Typical synthesis process was as follows: The polymer binders (SPPO+SPVC) (7 : 3 w/w) were dissolved in THF solvent. The mixture was mixed vigorously at room temperature to obtain a homogenous mixture. Then, a certain amount of $FeCl_3 \cdot 6H_2O$ was added to the above mixture under mechanical stirring at room temperature. To this solution, a desired amount of NH_4OH was then added dropwise, under stirring to reach a mild alkaline pH (~12). The mixture turned from yellow to brown, indicating the formation of FeOOH. For better dispersion of nanoparticles and breaking up their aggregates, the solution was sonicated for 10 min using an ultrasonic instrument. The mixture was then cast onto a clean and dry glass plate at 25 °C and was placed at room temperature. The samples were dried at ambient temperature up to complete solvent evaporation and membrane solidification. Then, the membranes were treated at 40 °C, 60 °C, 80 °C, 105 °C (every temperature lasted 2 h). Fig. 2 shows the schematic diagram for experimental procedure performed for preparation of ion-exchange nanocomposite membranes.

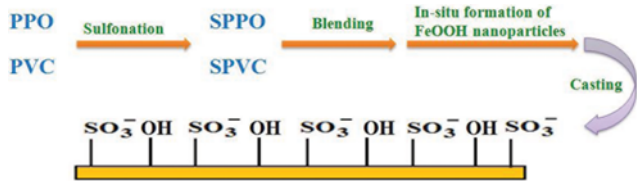

Fig. 2. Schematic diagram of ion-exchange nanocomposite membranes preparation.

Table 1. Compositions of casting solutions for the preparation of ion-exchange nanocomposite membranes

Membrane	$FeCl_3 \cdot 6H_2O$ (additive : total solid) (w/w)
Sample 1	(0.0 : 100)
Sample 2	(0.5 : 100)
Sample 3	(1 : 100)
Sample 4	(2 : 100)
Sample 5	(3 : 100)
Sample 6	(4 : 100)

Polymer binder (SPPO : SPVC) (w/w), (7 : 3); solvent (THF : Polymer binder) (v/w), (10 : 1)

As the final stage, the membranes were pretreated by immersing in HCl and NaCl solutions. A digital caliper device was applied for measuring membrane thickness, which confirmed that the thicknesses were maintained around about 30-36 micrometers. The compositions of casting solutions are shown in Table 1.

3. Characterization of Prepared Membranes

3-1. Ion-exchange Capacity (IEC), Swelling and Electrochemical Properties

For IEC measurements, membranes were first equilibrated in 50 ml of 1 M HCl solution for 24 h. After that, they were removed from the solution and washed with distilled water to eliminate excess of the acid. Then, membranes were immersed in 1 M NaCl to exchange hydrogen ions by the sodium ions. The amount of H^+ ions in the solution was determined by titration with 0.01 M NaOH. Ion-exchange capacity was expressed in milli-equivalents of H^+ per gram of dry membrane [32].

To evaluate the membrane swelling, samples were equilibrated in deionized water at room temperature for 24 h. The excess of water was dried with filter paper and the wet membranes were weighed and kept in the oven at 80 °C for 6 h and then weighed again. Uptake of water was determined by the mass difference between the wet and the dried membranes (after heating at 80 °C); water absorption was expressed in percentage [33,34].

The potential data were obtained using a two-compartment cell in which a circular membrane was placed between the two half-cells and was separated two NaCl solutions of concentrations 0.01 and 0.1 mol dm^{-3}. The membrane potential was measured using two calomel reference electrodes (through KCl bridges) with the aid of a digital auto multi-meter. The NaCl solutions in the compartments were stirred mechanically. The membrane potential developed between the solutions contacting with both membrane surfaces is expressed via the Nernst equation, which is employed to estimate the transport number of ions as follows:

$$E_m=(2t_i^m-1)\,(RT/nF)\ln(a_1/a_2) \quad (1)$$

where t_i^m is transport number of counter-ions in membrane phase, T is the temperature, R is gas constant, n is the electrovalence of counter-ion and a_1, a_2 are electrolyte activities in the solutions that are determined by Debye-Huckel limiting law. The higher transport number of the counter-ions t_i^m in a membrane indicates more permselectivity of the IEM. The ionic permselectivity of membranes also is quantitatively expressed on the basis of the counter-ion migration through the IEMs [35-38].

$$P_s=(t_i^m-t_0)/(1-t_0) \quad (2)$$

where, t_0 is the transport number of counter-ions in solution phase [39].

More conducting areas on the membrane surface can be supplied and its electrochemical properties may be enhanced by homogeneity and uniform distribution of functional groups on the membrane surface. The uniform electrical field intensity around the membrane can be strengthened and the concentration polarization phenomenon may be diminished by the presence of more conducting areas on the membrane surface. The concentration of fixed charge on the membrane surface (Y) has been demonstrated on the basis of the permselectivity as follows [40,41]:

$$Y=2C_{mean}P_s/\sqrt{1-P_s^2}$$

where C_{mean} is the mean concentration of electrolytes.

The test cell (Fig. 1) was used for the measurement of ionic permeability and the flux of ions. For this purpose, one side of the cell was filled with 0.1 M NaCl solution and another side with a 0.01 M solution. Using two stable platinum electrodes connected to the end of the compartments, a DC electrical potential (Dazheng, DC power supply, Model: PS- 302D) with optimal constant voltage was applied across the cell. By applying electrical potential during the experiment, cations (Na^+) permeate through the membrane to the cathodic compartment. Also, according to the following reactions, pH of this region is increased as a result of hydroxide ion production in the cathodic section. To calculate the transported cations through the membrane, the number of produced hydroxide ions in the cathodic section can be determined. So the pH change in the cathodic region is a measure of the ion permeation (Δn) through the membrane. The changes of pH versus time were measured using a digital pH meter (Jenway 3510).

$$2Cl^- \rightarrow Cl_2\uparrow + 2e^- \quad \text{(Anodic reaction)}$$
$$2H_2O + 2e^- \rightarrow H_2\uparrow + 2OH \quad \text{(Cathodic reaction)}$$

To establish the equilibrium condition in two solution-membrane interfacial sections and to minimize the effect of boundary layers, both sections were strongly mixed via magnetic stirrers [40,41].

The measurement of membrane resistance is important and it performs a significant role in the operative application of ion-exchange membranes. The membrane resistance measurement was performed using 0.5 M NaCl solution. The membrane sample was immersed in a 0.5 M NaCl solution for 24 h and was then washed with distilled water. First, the apparatus was assembled without a membrane. The cell compartments were filled with NaCl solution (0.5 M) at 25 °C and the electric resistance (R_2) was measured by

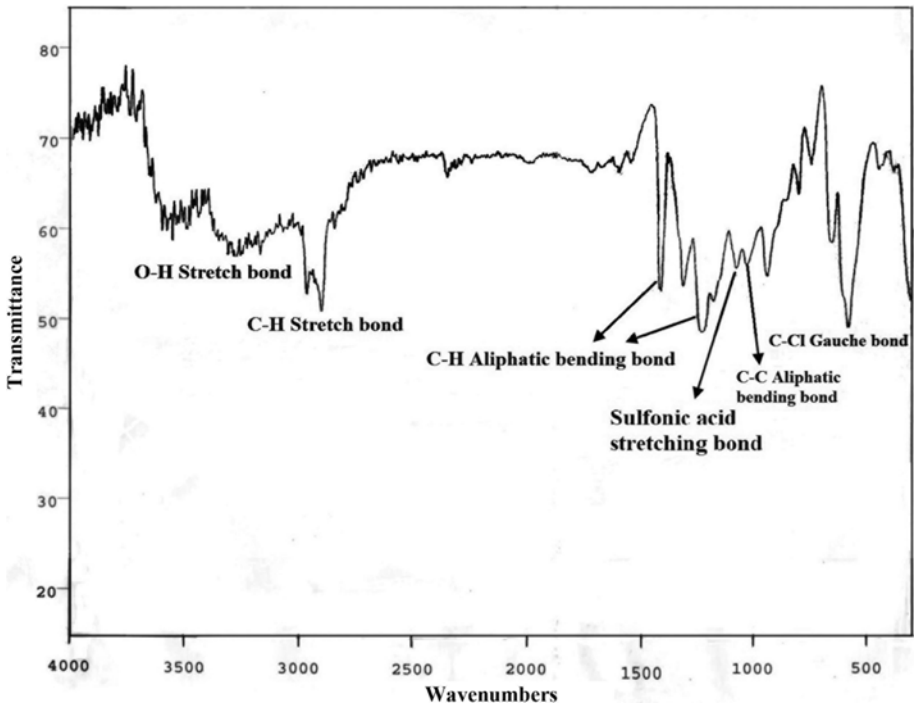

Fig. 3. The FTIR spectrum of SPVC.

an alternating current bridge with the frequency of 1,500 Hz (Audio signal generator, Electronic Afzar Azma Co. P.J.S). Then, the membrane was embedded into the cell and the electric resistance (R_1) was measured. The membrane resistance was determined from the difference between R_2 and R_1 ($R_m=R_1-R_2$). The specific resistance was expressed as follows [42]:

$$r=(R_mA) \tag{4}$$

where r is specific resistance and A is the surface area of the membrane.

The current efficiency (C.E) of the membranes is calculated using the following equation [43]:

$$C.E=\frac{F\times Z_i\times \Delta n}{\int_{t=0}^{t=t} Idt} \tag{5}$$

where Z_i is the valance of ion, Δn is transport number of moles, F is Faraday constant and I is the current intensity.

The measurements were performed three times for each sample and the average values were reported in order to minimize the experimental errors.

3-2. Membrane Oxidative Stability

To evaluate the oxidative stability of prepared membranes, they were soaked into 3% H_2O_2 aqueous solution containing 4 ppm Fe^{3+} at 25 °C for 60 h. The weight of the dried membranes (dried at 65 °C for 4 h) before and after the experiment was measured (using Mettler Toledo Group, Model: AL204). The percentage of the reduced weight is attributed to the oxidative stability of membrane [23].

3-3. Mechanical Properties

The mechanical properties of the membranes were measured by means of a tear test in a wet state at room temperature. All samples were cut into a rectangular shape with 50 mm×5 mm dimension. For obtaining precise results, at least three specimens from each sample were tested and the average value was reported.

RESULTS AND DISCUSSION

1. Membrane Structure-chemistry

Fig. 3 shows the FT-IR spectrum of the sulfonated PVC. The wide peak at around a wave number of 3,450-3,500 cm^{-1} corresponds to the O-H hydroxyl bond, and can be attributed to water adsorbed by SPVC. Absorptions in the range of 2,800-3,000 cm^{-1} correspond to C-H bond. The C-C bending bond of the PVC backbone chain occurs in the range of 1,000-1,100 cm^{-1}. Absorption peak at 610 cm^{-1} is related to C-Cl gauche bond. The peak around 1,065 cm^{-1} is assigned to stretching of the sulfonic acid group. Other details of FT-IR spectrum are shown in Fig. 3.

Fig. 4 shows the ATR-FTIR spectra of prepared membranes. Absorption peak at 1,467 cm^{-1} is related to C=C bond of aromatic rings, and absorption at 1,131 cm^{-1} is responsible for C-O bond. A peak at 1,602 cm^{-1} corresponds to S=O bond in polymer matrix. Absorptions at 2,937 and 3,061 cm^{-1} are responsible for aliphatic and aromatic bonds, respectively. Stretching vibration of O-H bond appears at 3,457 cm^{-1}. Absorption peaks at 615 cm^{-1} and 675 cm^{-1} (Fig. 4(b)) related to Fe-O bond approve the presence of FeOOH nanoparticles in the polymeric matrix.

The XRD pattern of SPPO+SPVC/FeOOH nanocomposite is shown in Fig. 5. Pure polymeric matrix has a semi-crystalline structure that just shows a broad peak around 20-30 degrees. While, the inorganic FeOOH nano-filler has a pure crystalline structure. Peaks of ferric oxyhydroxide have suitable agreement with refer-

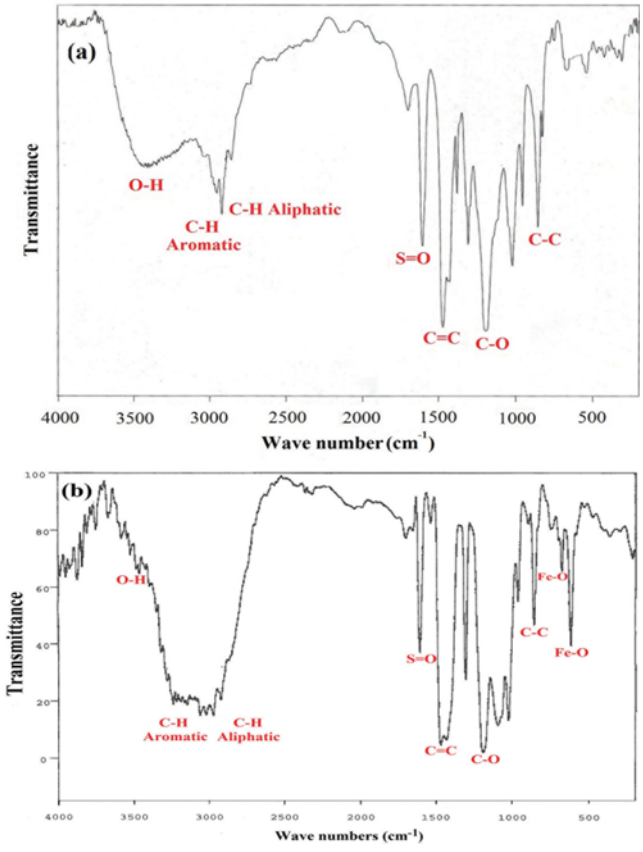

Fig. 4. FT-IR spectra of the prepared membranes (a) SPPO+SPVC (b) SPPO+SPVC/FeOOH.

ence peaks (JCPDS: 81-0464, crystal system: orthorhombic, Geothite, space group: Pbnm) [44] appearing in the XRD pattern of the nanocomposite that confirms the existence of FeOOH in the polymeric matrix. No other peak related to impurity was observed and narrow peaks confirmed crystallinity of the inorganic phase. The crystallite size evaluation was also performed using the Scherrer equation.

$$Dc=0.9\lambda/\beta\cos\theta \quad (6)$$

where β is the width of the observed diffraction peak at its half maximum intensity (FWHM) and λ is the X-ray wavelength (CuKα radiation, equals to 0.154 nm). The calculated crystallite size is about 14 nm.

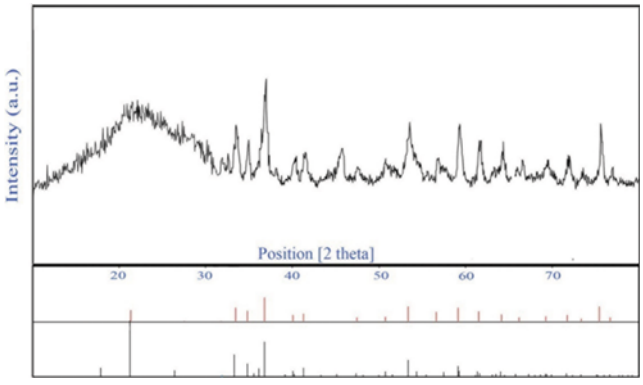

Fig. 5. XRD pattern of SPPO+SPVC/FeOOH nanocomposite.

2. Membrane Structure-morphology

To evaluate the morphology of membrane matrix, scanning electron microscopy investigations were carried out. The SEM images of the surface and cross section of prepared membranes, presented in Figs. 6 and 7, respectively, confirm the suitable dispersion of nanoparticles in the polymeric matrices (except sample 6 with 4 wt% additive loading).

3. Swelling and Ion-exchange Capacity (IEC)

The results (Table 2) indicated that swelling of prepared membranes slightly increased with the enhancement of FeOOH nanoparticle loading. The small size and the large surface area of the in-situ synthesized FeOOH nanoparticles will expose a large number of hydroxyl groups at the surface, which should be the reason for the large amount of hydrogen bonded water and the physically adsorbed water [30]. Moreover, with more filler loadings, voids and cavities are formed between inorganic nanoparticles and polymer binder region due to heterogeneity [45], which increases the amount of water content in the nanocomposite membranes. Therefore, more water is embedded by the membrane structure with increase in additive loading. Moreover, the high content of the bonded water means the presence of abundant surface hydroxyl groups, which is in favor of the adsorption characteristics.

Table 2 shows the ion-exchange capacity of the prepared nanocomposite membranes. The results indicated that the increment of additive loading up to 3%wt (sample 5) in the casting solution initially led to an improvement in ion-exchange capacity in prepared membranes. The finding could be attributed to FeOOH nanoparticles produced on the membrane surface that might provide more active sites for the ion adsorption due to adsorption characteristic of FeOOH nanoparticles [46]. The suitable dispersion of in-situ synthesized FeOOH nanoparticles provides more accessible active sites for suitable interaction between ions and membrane surface and so enhances the ion exchange feasibility. However, the highest IEC was not observed at the highest additive content (sample 6). This finding may be probably owing to formation of numerous FeOOH nanoparticles on the membrane's surface which tend to aggregation (Fig. 6(e) and Fig. 7(b)), finally leading to reduction of the accessibility of ion-exchange functional groups by their surrounding, which in turn leads to IEC decrease.

4. Fixed Ion Concentration (F.I.C)

Membrane efficiency can be achieved by the resultant effects of the IEC and water content. The fixed ion concentration (F.I.C.) or the equivalent of functional group per absorbed water can be used to achieve this resultant effect. Fig. 8 shows the fixed ion concentration of the prepared membranes. Sample 5 has exhibited a suitable F.I.C compared to the other prepared membranes. This fact is attributable to the higher relative IEC and suitable swelling for this sample.

5. Membrane Potential, Surface Charge Density, Permselectivity and Transport Number

The membrane potential of the prepared membranes is shown in Fig. 9. The thickness of the membranes was about 30-36 micrometers (Table 2). At first, membrane potential was improved with the increase of additive loading (up to 3%wt) (sample 5) in the pre-

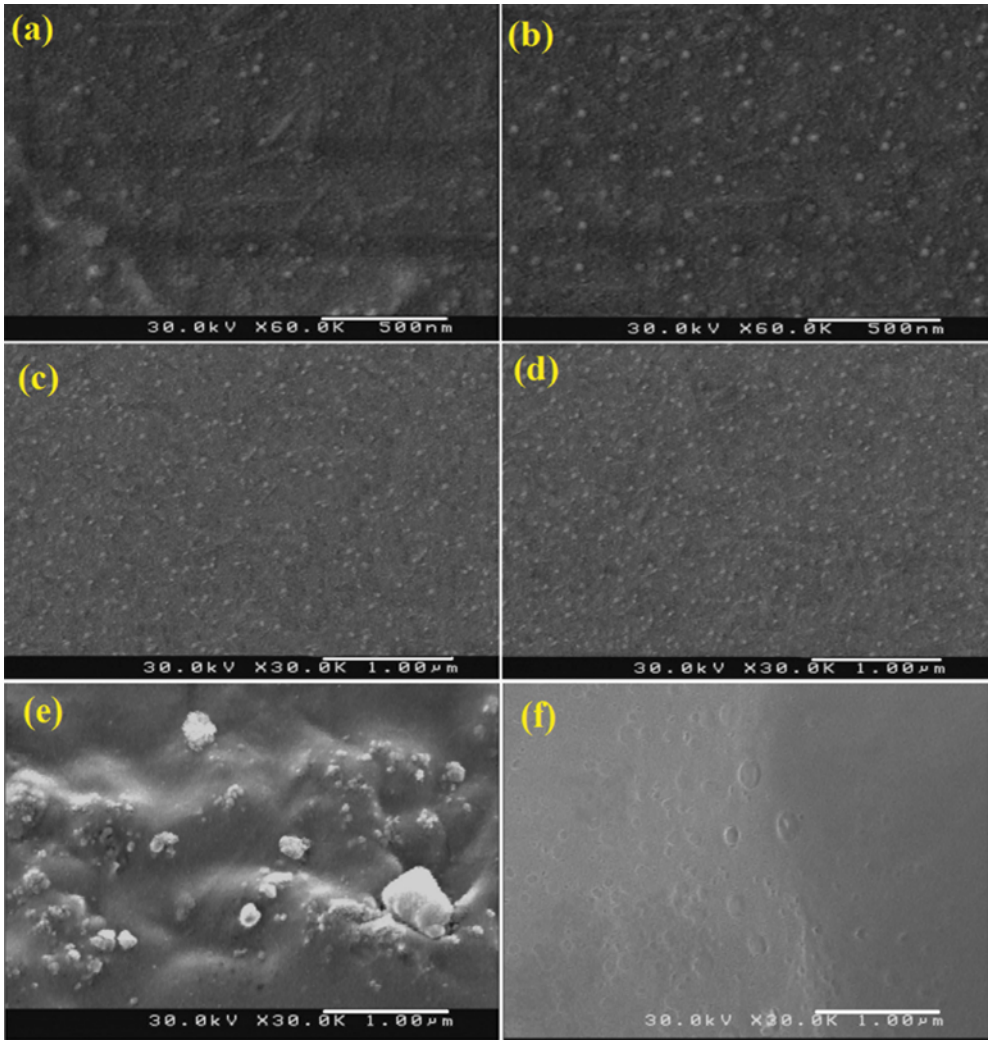

Fig. 6. SEM images of prepared membranes with various loadings of additive (a) 0.5 wt%; (b) 1 wt%; (c) 2 wt%; (d) 3 wt%; (e) 4 wt%; (f) 0% (without additive).

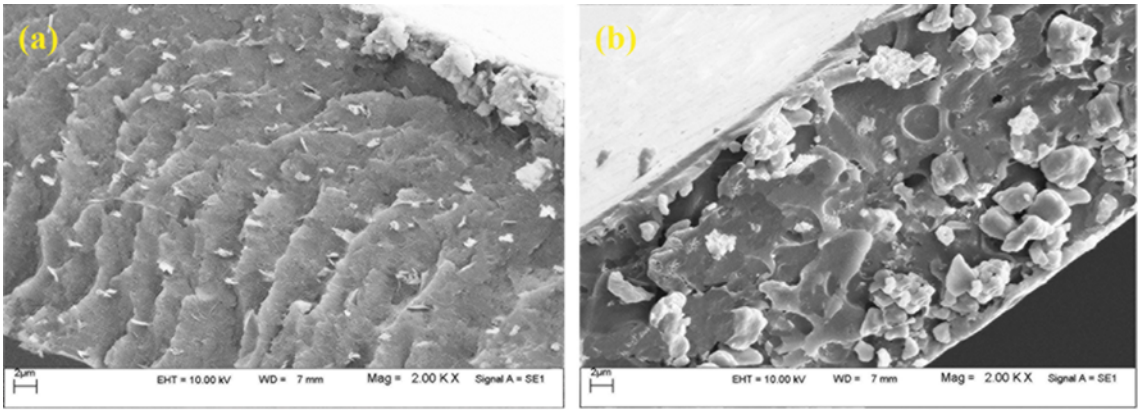

Fig. 7. SEM cross section images of prepared nanocomposite membranes with various loadings of additive (a) 3 wt%; (b) 4 wt%.

pared membranes.

The increase in membrane F.I.C value leads to improvement in surface charge density (Fig. 9), which provides additional conducting regions for the membrane. This leads to an improvement in the Donnan exclusion, which is responsible for the increment in membrane potential [47,48]. Also, the existence of greater conducting regions on the surface of membrane can strengthen the intensity of uniform electrical field around the membrane and decrease

Table 2. Ion exchange capacity and swelling of prepared membranes

Sample's number	IEC (meq/gr)	Swelling (%)	Membranes thickness (μm)
1	0.285	14.82 (±0.2)	34
2	0.310	15.53 (±0.3)	35
3	0.354	17.21 (±0.8)	31
4	0.416	19.06 (±0.8)	30
5	0.521	23.12 (±1)	32
6	0.383	35.32 (±1.5)	36

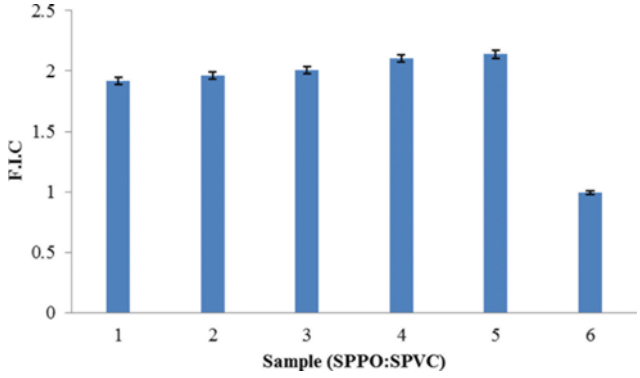

Fig. 8. Fixed ion concentration of prepared membranes.

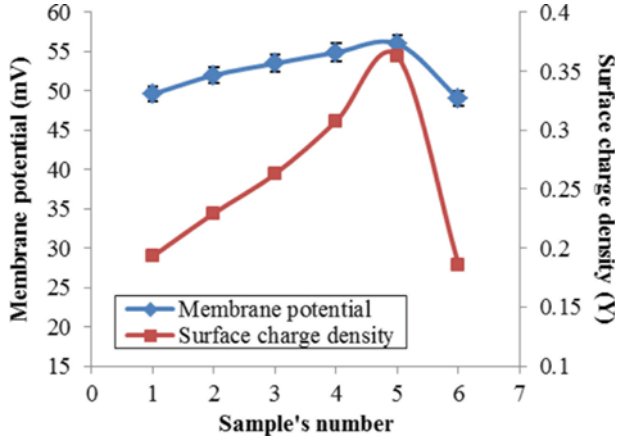

Fig. 9. The effect of additive loading on membrane potential and surface charge density of the prepared membranes.

the concentration polarization phenomenon [49]. The membrane potential was decreased again with more increment in additive concentration from 3 to 4 wt% due to lower membrane surface charge density and fixed ion concentration.

The permselectivity and transport number of membranes are depicted in Fig. 10. At first, both increased with the increment of additive loading to 3 wt% (sample 5) in the casting solution. This trend can be explained with respect to the increment in surface charge density with higher control of pathways for ions traffic. With the increase of additive concentration (up to 3 wt%), the ionic pathways in the membrane are partially filled via FeOOH nanoparticles with high surface hydroxyl groups [30], and so passages are

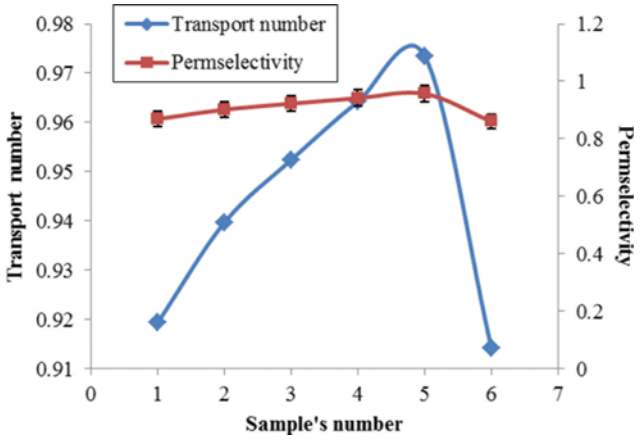

Fig. 10. The permselectivity and transport number of prepared membranes with various additive loadings.

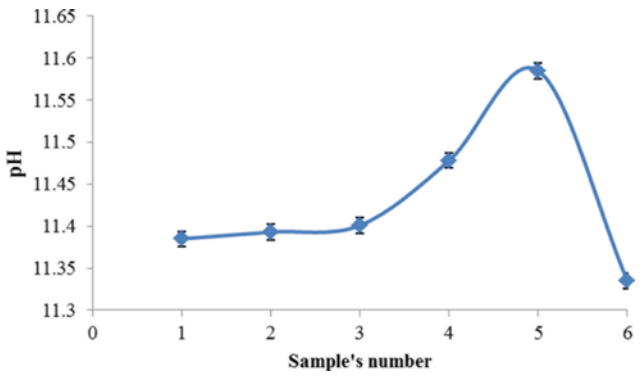

Fig. 11. The variation of pH in cathodic section at the end of experiment (initial pH=7.536 at ambient temperature).

narrowed by them as space limiting factors. This leads to increased control of the ionic sites on ions transit and enhances the membrane permselectivity. The permselectivity and transport number were diminished again with more additive loading (sample 6) due to higher water content and lower membrane IEC, which both reduce the concentration of ionic sites in membrane network. This simplifies the passing of co-ions across the membrane and decreases the selectivity. Moreover, higher increment in additive content reduces the membrane selectivity due to enhancement of nanoparticles density in the casting solution, which leads to discontinuity of polymer chains binder. In addition, high water content facilitates counter- and co-ions transport but reduces the ion selectivity.

6. Ionic Permeability and Flux

During the experiment, ions permeate through the membrane and reach the concentration section. According to occurred reactions in the cathodic and anodic sections, the amount of transported Na^+ ions through the membrane to concentration compartment is equal to the produced hydroxide ions in the cathodic section. Therefore, the permeation of ions through the membrane can be calculated from the conductivity variations or pH changes in cathodic region [40]. The ionic permeability and flux results were deduced from pH changes in the cathodic region. The pH values in the cathodic section (at the end of experiment) are shown in Fig. 11.

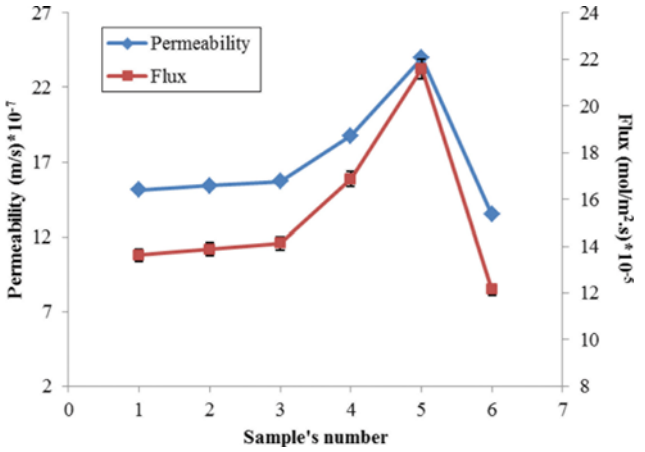

Fig. 12. The ionic permeability and flux of prepared cation-exchange nanocomposite membranes with various ratios of additive loadings in monovalent ionic solutions.

Results (Fig. 12) showed that the ionic permeability and flux were first increased with increment in additive loading up to 3 wt% (sample 5) in the casting solution. This is essentially because of the increased IEC and swelling in the prepared membranes due to in-situ formation of inorganic nanoparticles. These effects lead to increased penetration rate of counter-ions into the membrane and facilitate the migration of ions through the membrane and subsequently enhance the flux.

Composite membranes with different porosities were obtained as a result of evident interfacial interaction of polymer network with various loadings of inorganic phase [34]. Decreasing the ionic flux in the case of sample 6 is due to surface pore blockage by nanoparticles and decline of surface pore size [50]. This directly affects the ion permeation rate through the membrane. Also, this can be attributed to the decreased F.I.C and also increased tortuosity of this nanocomposite sample, which leads to restricted diffusion of counter-ions. Note that at higher additive loading (sample 6) the FeOOH nanoparticles tend to be accumulated in the membrane structure (Fig. 6(e) and Fig. 7(b)), and thus tortuosity is increased due to the more polymer-filler aggregate interaction. The proposed mechanism of nanoparticle aggregation is shown schematically in

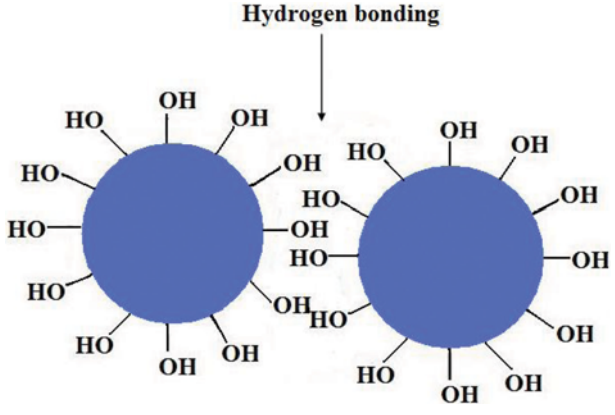

Fig. 13. Schematic illustration of nanoparticles aggregation.

Table 3. The effect of additive loading on weight loss in the oxidative stability test

Sample's number	Weight loss (%)
1	13.08 (±0.2)
2	14.22 (±0.2)
3	14.89 (±0.3)
4	16.21 (±0.5)
5	17.53 (±0.5)
6	19.93 (±0.8)

Fig. 13. The presence of the hydroxyl groups on the surface of FeOOH nanoparticles is the main reason for their tendency to attract one another through hydrogen bonds and, therefore, become agglomerated.

7. Membrane Oxidative Stability

To evaluate the oxidative durability, the prepared membranes were immersed in an oxidant aqueous solution (H_2O_2 aqueous solution containing Fe^{3+}). The oxidative stabilities are presented in Table 3. The results indicated that the FeOOH embedded membranes cause oxidative stabilities to decrease. This may be due to the adsorption features of the nanocomposite membranes. The existence of hydroxyl groups on the surface of FeOOH nanoparticles leads to enhanced wettability of the membrane interface or matrix. The increasing of wettability for the prepared nanocomposite membranes results in higher oxidant diffusion in the membrane network and more weight loss during the oxidative stability test. Also, IEC values were changed after oxidative stability tests. Therefore, due to presence of iron in the nanocomposite matrix, the prepared membranes are useless in an environment containing H_2O_2, which causes the gradual degradation of polymer chain.

8. Electrical Resistance

The effect of additive loading on specific electrical resistance of prepared membranes is given in Table 4. The results clearly indicate that electrical resistance was decreased with increment in additive loadings to 3 wt%. The swelling capacity of the membrane affects not only dimensional durability but also electrical resistance. The higher the tendency of the membrane to water, the lower the resistance to ion transport. Also, electrical resistance decline is assigned to the increased IEC of nanocomposite membranes, which increases cation interaction with membrane surface and facilitates ion permeation. For sample 6 with 4 wt% additive loading, the specific electrical resistance was enhanced due to formation of tortuous and narrow ionic transfer channels in membrane structure (as mentioned before) and also isolation of ionic functional groups

Table 4. The specific electrical resistance of prepared membranes with various ratios of additive content

Sample's number	Specific resistance (Ω cm^2)
1	62.98 (±1.5)
2	33.65 (±0.8)
3	31.23 (±0.9)
4	28.12 (±0.9)
5	25.21 (±1)
6	45.37 (±1.5)

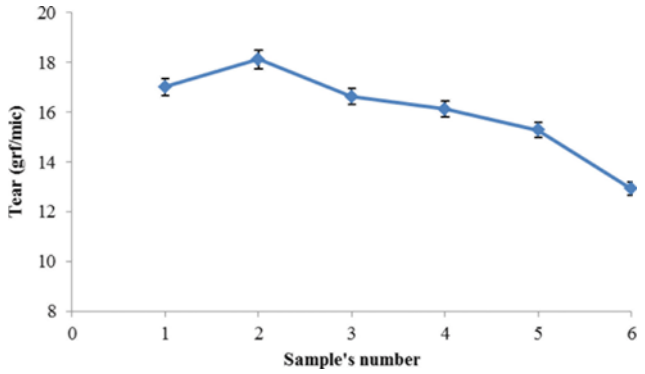

Fig. 14. The effect of additive loading on mechanical property of the prepared membranes.

by FeOOH nanoparticles, which in turn leads to IEC decrease. These decrease the ion transport and so enhance the specific electrical resistance. However, the nanocomposite membranes showed lower specific electrical resistance compared to pristine membrane (sample 1).

9. Mechanical Properties and Current Efficiency

Mechanical properties of the prepared membranes were evaluated by tear test. The effect of additive loading on mechanical property of prepared membranes is shown in Fig. 14. The obtained results showed that the mechanical strength initially improved with increase in additive content up to 0.5 wt% (sample 2). It can be attributed to large interface between the FeOOH nanoparticles and polymeric matrices, resulting from hydrophilic surface of the FeOOH nanoparticles and from strong interaction between the FeOOH nanoparticles and polymer [51]. As the additive content increased from sample 2 to 6, the mechanical strength generally diminished. This is due to discontinuity of binder, which tends to produce discrete phase. These composite membranes (samples 3 to 6) were more brittle than the pristine membrane (sample 1) because of the incorporation of inorganic FeOOH nanoparticles. As previously mentioned, the porosity of the composite membranes can be attributed to the polymer-filler interfacial gap. During the preparation process, the evaporation of solvent introduces voids and cavities between the polymer binder and nanoparticles. In addition, infusible and insoluble inorganic nanoparticles are unable to form a film.

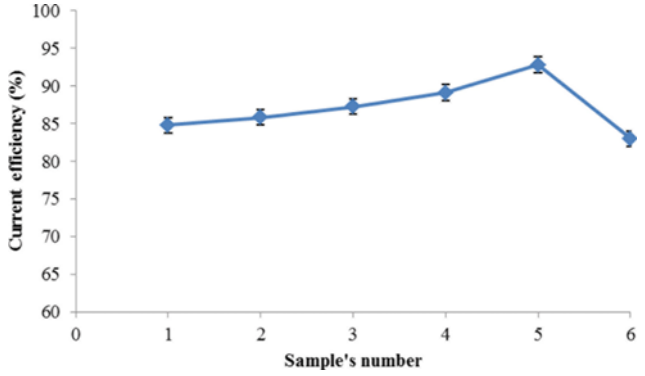

Fig. 15. Current efficiency of the prepared membranes.

Therefore, with the enhancement of filler loading, crack development becomes facile and a fragile and weaker membrane will be obtained [8,52].

Fig. 15 presents the current efficiency of the prepared membranes. The results indicate that current efficiency was increased as a result of increase in ionic flux and permeability with increment in additive loadings to 3 wt% (sample 5) in the prepared membranes. Moreover, the current efficiency was decreased with higher additive loading from 3 to 4 wt%. As expected, the membrane with 4 wt% (sample 6) exhibited lower current efficiency compared to others. However, it can be due to low values of ionic permeability and transport number in the mentioned membrane.

CONCLUSION

SPPO+SPVC/FeOOH nanocomposites have been successfully prepared by a one-step synthetic method in the presence of Fe^{3+} and OH^-. We developed a facile procedure for the in-situ formation of FeOOH on polymer binders' matrix (SPPO+SPVC) with high uniformity. The SEM images showed uniform nanoparticles distribution and also relatively uniform surface for the prepared nanocomposite membranes. Microstructure, physicochemical and electrochemical properties including IEC, swelling, membrane potential, transport number, permselectivity, specific resistance, ionic permeability, flux of ions, current efficiency, mechanical properties and membrane oxidative stability of the prepared nanocomposite membranes have been characterized precisely. It was found that FeOOH nanoparticles could affect overall physicochemical and electrochemical properties. Moreover, obtained results indicated that prepared membranes with additive concentrations up to 3%wt showed higher IEC, F.I.C, surface charge density, membrane potential, transport number, permselectivity, current efficiency, ionic flux and permeability compared to pristine membrane (sample 1). Furthermore, all modified membranes containing nanoparticles exhibited lower specific electrical resistance compared to pristine membrane. This work introduces a cation-exchange nanocomposite membrane containing 3 wt% additive loading (sample 5), with suitable IEC, FIC, transport number, permselectivity, ionic flux, permeability, current efficiency, oxidative stability and low specific electrical resistance as a new superior and applicable membrane.

ACKNOWLEDGEMENT

The authors are thankful to Laboratory of Functional Membranes (University of Science and Technology of China) for providing PPO.

NOMENCLATURE

A : membrane surface area [m^2]
a : milli-equivalent of ion-exchange groups in membrane [meq]
a_1, a_2 : ions electrolytic activities
C.E : current efficiency
C_{mean} : mean concentration of electrolytes [M]
d : membrane thickness [m]
E_m : membrane potential [mV]

F : faraday constant
FT-IR : fourier transform infrared spectroscopy
I : current intensity [A]
IEC : ion-exchange capacity
IEMS : ion-exchange membranes
n, Z_i : electrovalence of ion
P_s : membrane ionic permselectivity
R : universal gases constant [J mol^{-1} K^{-1}]
r : specific electrical resistance [Ω cm^2]
R_1 and R_2 : electrical resistance [Ω]
R_m : membrane resistance [Ω]
SEM : scanning electron microscope
SPPO : sulfonated poly (2,6-dimethyl-1,4-phenylene oxide)
SPVC : sulfonated polyvinylchloride
T : temperature [K]
t : time [min]
THF : tetrahydrofuran
t_i^m; t_0 : transport number of counter ions in membrane phase; in solution
Y : concentration of fixed charge on the membrane surface
Δn : number of transported moles through membrane

REFERENCES

1. X. Zuo, S. Yu, X. Xu, J. Xu, R. Bao and X. Yan, *J. Membr. Sci.*, **340**, 206 (2009).
2. L. J. Banasiak, B. Van der Bruggen and A. I. Schafer, *Chem. Eng. J.*, **166**, 233 (2011).
3. F. Karimi, S. N. Ashrafizadeh and F. Mohammadi, *Chem. Eng. J.*, **183**, 402 (2012).
4. H. J. Lee, M. K. Hong and S. H. Moon, *Desalination*, **284**, 221 (2012).
5. J. Luo, C. Wu, T. Xu and Y. Wu, *J. Membr. Sci.*, **366**, 1 (2011).
6. M. C. Martí-Calatayud, D. C. Buzzi, M. García-Gabaldón, A. M. Bernardes, J. A. S. Tenório and V. Pérez-Herranz, *J. Membr. Sci.*, **466**, 45 (2014).
7. S. H. Moon and S. H. Yun, *Curr. Opin. Chem. Eng.*, **4**, 25 (2014).
8. P. V. Vyas, B. G. Shah, G. S. Trivedi, P. Ray, S. K. Adhikary and R. Rangarajan, *J. Membr. Sci.*, **187**, 39 (2001).
9. P. V. Vyas, B. G. Shah, G. S. Trivedi, P. Ray, S. K. Adhikary and R. Rangarajan, *React. Funct. Polym.*, **44**, 101 (2000).
10. C. Vogel and J. Meier-Haack, *Desalination*, **342**, 156 (2014).
11. K. A. Mauritz, *Mater. Sci. Eng. C*, **6**, 121 (1998).
12. M. L. Sforca, I. V. P. Yoshida and S. P. Nunes, *J. Membr. Sci.*, **159**, 197 (1999).
13. R. K. Nagarale, G. S. Gohil, V. K. Shahi, G. S. Trivedi and R. Rangarajan, *J. Colloid Interface Sci.*, **277**, 162 (2004).
14. M. M. A. Khan and Rafiuddin, *J. Appl. Polym. Sci.*, **124**, 338 (2012).
15. P. Xu, G. M. Zeng, D. L. Huang, C. L. Feng, S. Hu, M. H. Zhao, C. Lai, Z. Wei, C. Huang, G. X. Xie and Z. F. Liu, *Sci. Total Environ.*, **424**, 1 (2012).
16. L. Y. Ng, A. W. Mohammad, C. P. Leo and N. Hilal, *Desalination*, **308**, 15 (2013).
17. A. R. Khodabakhshi, S. S. Madaeni, T. W. Xu, L. Wu, C. Wu, C. Li, W. Na, S. A. Zolanvari, A. Babayi, J. Ghasemi, S. M. Hosseini and A. Khaledi, *Sep. Purif. Technol.*, **90**, 10 (2012).
18. T. W. Xu, W. H. Yang and B. L. He, *Chin. J. Polym. Sci.*, **20**, 53 (2002).
19. T. W. Xu, D. Wu and L. Wu, *Prog. Polym. Sci.*, **33**, 894 (2008).
20. H. Yu and T. W. Xu, *J. Appl. Polym. Sci.*, **100**, 2238 (2006).
21. D. Wu, L. Wu, J. J. Woo, S. H. Yun, S. J. Seo, T. W. Xu and S. H. Moon, *J. Membr. Sci.*, **348**, 167 (2010).
22. X. Zhang, Y. Chen, A. H. Konsowa, X. Zhu and J. C. Crittenden, *Sep. Purif. Technol.*, **70**, 71 (2009).
23. L. Xu and H. K. Lee, *J. Chromatogr. A*, **1216**, 6549 (2009).
24. H. M. Xiao, W. D. Zhang and S. Y. Fu, *Compos. Sci. Technol.*, **70**, 909 (2010).
25. H. J. Song, L. Liu, X. H. Jia and C. Y. Min, *J. Nanopart. Res.*, **14**, 1 (2012).
26. B. Wang, H. B. Wu, L. Yu, R. Xu, T. T. Lim and X. W. Lou, *Adv. Mater.*, **24**, 1111 (2012).
27. F. M. Peng, T. Luo, L. G. Qiu and Y. P. Yuan, *Mater. Res. Bull.*, **48**, 2180 (2013).
28. C. H. Xu, J. J. Shi, W. Z. Zhou, B. Y. Gao, Q. Y. Yue and X. H. Wang, *Chem. Eng. J.*, **187**, 63 (2012).
29. Z. Wang, Y. Ma, H. He, C. Pei and P. He, *Appl. Surf. Sci.*, **332**, 456 (2015).
30. P. Y. Wu, Y. Jia, Y. P. Jiang, Q. Y. Zhang, S. S. Zhou, F. Fang and D. Y. Peng, *J. Environ. Chem. Eng.*, **2**, 2312 (2014).
31. T. W. Xu, W. H. Yang and B. L. He, *Chem. Eng. Sci.*, **56**, 5343 (2001).
32. H. Strathmann, *Membrane Separations Technology: Principles and Applications*, Elsevier, New York (1995).
33. R. Scherer, A. M. Bernardes, M. M. C. Forte, J. Z. Ferreira and C. A. Ferreira, *Mater. Chem. Phys.*, **71**, 131 (2001).
34. W. Cui, J. Kerres and G. Eigenberger, *Sep. Purif. Technol.*, **14**, 145 (1998).
35. R. K. Nagarale, V. K. Shahi and R. Rangarajan, *J. Membr. Sci.*, **248**, 37 (2005).
36. G. S. Gohil, V. V. Binsu and V. K. Shahi, *J. Membr. Sci.*, **280**, 210 (2006).
37. J. Schauer, V. Kudela, K. Richau and R. Mohr, *Desalination*, **198**, 256 (2006).
38. L. Lebrun, E. Da Silva, G. Pourcelly and M. Métayer, *J. Membr. Sci.*, **227**, 95 (2003).
39. D. R. Lide, *CRC Handbook of Chemistry and Physics*, CRC Press, Boca Raton (2010).
40. A. Zendehnam, M. Rabieyan, S. M. Hosseini and S. Mokhtari, *Korean J. Chem. Eng.*, **32**, 501 (2015).
41. G. J. Hwang, S. G. Lim, S. Y. Bong, C. H. Ryu and H. S. Choi, *Korean J. Chem. Eng.*, **32**, 1896 (2015).
42. Y. Tanaka, *Ion exchange membranes: Fundamentals and applications, Membrane Science and Technology Series,* vol. 12, Elsevier, Netherlands (2007).
43. R. K. Nagarale, G. S. Gohil and V. K. Shahi, *Adv. Colloid Interface Sci.*, **119**, 97 (2006).
44. G. Nabiyouni and D. Ghanbari, *J. Appl. Polym. Sci.*, **125**, 3268 (2012).
45. M. Y. Kariduraganavar, R. K. Nagarale, A. A. Kittur and S. S. Kulkarni, *Desalination*, **197**, 225 (2006).
46. W. Wan, T. J. Pepping, T. Banerji, S. Chaudhari and D. E. Giammar, *Water Res.*, **45**, 384 (2011).
47. V. K. Shahi, R. Prakash, G. Ramachandraiah, R. Rangarajan and D. Vasudevan, *J. Colloid Interface Sci.*, **216**, 179 (1999).

48. R. K. Nagarale, V. K. Shahi, S. K. Thampy and R. Rangarajan, *React. Funct. Polym.*, **61**, 131 (2004).
49. M. S. Kang, Y. J. Choi, I. J. Choi, T. H. Yoon and S. H. Moon, *J. Membr. Sci.*, **216**, 39 (2003).
50. S. A. Patil and T. M. Aminabhavi, *J. Membr. Sci.*, **281**, 95 (2006).
51. R. Shahabadi, M. Abdollahi and A. Sharif, *Int. J. Hydrogen Energy*, **40**, 3749 (2015).
52. V. K. Shahi, G. S. Trivedi, S. K. Thampy and R. Rangarajan, *J. Colloid Interface Sci.*, **262**, 566 (2003).